Published in final edited form as:

Mol Cell Neurosci. 2006 ; 32(0): 82–90. doi:10.1016/j.mcn.2006.02.004.

Novel β subunit mutation causes a slow-channel syndrome by enhancing activation and decreasing the rate of agonist dissociation

Manuel F. Navedo[a], **José A. Lasalde-Dominicci**[b], **Carlos A. Báez-Pagán**[b], **Luzed Díaz-Pérez**[b], **Legier V. Rojas**[c], **Ricardo A. Maselli**[d], **Julie Staub**[e], **Kelly Schott**[e], **Roberto Zayas**[e], and **Christopher M. Gomez**[e,*]

[a]Department of Physiology and Biophysics, University of Washington, Seattle, WA 98195-7290, USA

[b]Department of Biology, University of Puerto Rico, San Juan, PR 00931, USA

[c]Department of Physiology, Universidad Central del Caribe, Bayamón, PR 00960, USA

[d]Section of Neuroscience, University of California, Davis, CA 95616, USA

[e]Department of Neurology and Neuroscience, MMC 295 420 Delaware St. SE University of Minnesota, Minneapolis, MN 55455, USA

Abstract

We traced the cause of a slow-channel syndrome (SCS) in a patient with progressive muscle weakness, repetitive compound muscle action potential and prolonged low amplitude synaptic currents to a V → F substitution in the M1 domain of the β subunit (βV229F) of the muscle acetylcholine receptor (AChR). In vitro expression studies in *Xenopus* oocytes indicated that the novel mutation βV229F expressed normal amounts of AChRs and decreased the ACh EC_{50} by 10-fold compared to wild type. Kinetic analysis indicated that the mutation displayed prolonged mean open duration and repeated openings during activation. Prolonged openings caused by the βV229F mutation were due to a reduction in the channel closing rate and an increase in the effective channel opening rate. Repeated openings of the channel during activation were caused by a significant reduction in the agonist dissociation constant. In addition, the βV229F mutation produced an increase in calcium permeability. The kinetic and permeation studies presented in this work are sufficient to explain the consequences of the βV229F mutation on the miniature endplate currents and thus are direct evidence that the βV229F mutation is responsible for compromising the safety margin of neuromuscular transmission in the patient.

Introduction

The slow-channel syndrome (SCS) is a disorder characterized by muscular weakness and fatigability due to gain-in-function mutations in the subunits of the muscle acetylcholine receptor (AChR) of the neuromuscular junction (NMJ). SCS-associated mutations

*Corresponding author. gomez001@tc.umn.edu (C.M. Gomez).

dramatically alter the function of the AChRs and thus impair neuromuscular transmission (Engel et al., 1996; Muley and Gomez, 2002). Characterization of the kinetic abnormalities produced by the SCS-associated mutations has provided insightful information about the consequences of the mutations on synaptic transmission and into the structure and function of the AChR.

Several molecular mechanisms underlying the SCS have been identified. For example, SCS mutations in the extracellular domain of the α subunit, which forms the presumed ligand binding pocket, cause increased ACh affinity leading to repeated openings of the channel during activation and to a slower decay of the synaptic current (Sine et al., 1995; Croxen et al., 1997). Numerous SCS mutations in the M2 domain, which line the water-filled ion channel pore, have a pronounced effect on ion channel gating (closing and opening rate constants), causing prolongation of single-channel open times, of activation episodes and, as a consequence, of synaptic decay phases (Milone et al., 1997; Gomez et al., 2002b; for a review, see Engel et al., 2003). More recently, SCS mutations in the M1 domain of the α and ε subunits were found to slow the rate of agonist unbinding, resulting in an increase in the number of re-openings per activation episode and prolonged activation events (Wang et al., 1997; Hatton et al., 2003). This kinetic abnormality was enough to explain the prolonged decay time of the synaptic current observed in the patients. These results indicated a modulatory role of the M1 domain in structures that couple ligand binding to the channel gate.

Here, we described a novel form of SCS cause by a βV229F mutation in the M1 domain of the AChR β subunit. In vitro expression studies in *Xenopus* oocytes indicated that the βV229F mutation did not affect expression levels of the receptor, but significantly increased the duration of the channel opening episodes. Kinetic analysis revealed that the prolonged open channel episodes were the result of a significant reduction in the agonist dissociation and closing rates constants, combined with an increase in the effective opening rate of the channel. This indicated a contribution of position βV229 to channel gating and an apparent allosteric modulation of the binding site. These observations are somewhat unexpected since other SCS-M1 domain mutations mainly affect the agonist dissociation constant with little or no effect on the other rate constants. Nevertheless, the kinetic and permeation studies presented in this study are direct and irrefutable evidence indicating that the βV229F mutation is responsible for compromising the safety margin of neuromuscular transmission in the patient.

Results

Clinical and electrophysiological studies

The proband of Kindred UM7 (Fig. 2A) was a 75-year-old male (UM7:II3) who noted slowly progressive weakness and later atrophy of hand and forearm muscles in his teens, leg weakness in his 60s and neck weakness at 70. His mother and two uncles (UM7:I2–I4) had similar symptoms. His niece (UM7:III1) had intermittent weakness since her teens and developed slowly progressive hand weakness in her 40s. Two sons, one asymptomatic at age 53 (UM7:III3) and one with forearm weakness since age 50 (UM7:III4), had mild eye muscle weakness when examined. Compound muscle action potentials recorded in hand or

forelimb muscles showed hallmark repetitive responses to single stimuli and evidence of impaired neuromuscular transmission in the proband, two of his sons and his niece, suggesting the presence of a dominantly inherited congenital myasthenic syndrome. In vitro microelectrode studies performed on the left anconeus muscle of the proband's son (UM:III4) at age 48 revealed that the quantal release by the nerve impulse was reduced by 40%. In addition, the amplitude of the miniature endplate current (MEPC) was reduced by 61% and MEPC were prolonged and decayed bi-exponentially, with one open time component close to normal and one significantly prolonged (Fig. 1; Table 1). These results suggested a severe reduction in safety factor of neuromuscular transmission caused by a kinetic disorder of the AChR. These characteristics were not observed in 82 individuals used as control.

Genetic studies

We identified a G-to-T transversion at position 770 of the β subunit gene coding region, predicting the missense mutation βV229F, in genomic DNA from affected members of this kindred (Fig. 2B). Patient 7-1, two of his sons, his niece and one of her sons were heterozygous for this mutation (Fig. 2A). His third son and one great nephew, who had no neuromuscular symptoms, only had the normal sequence (Fig. 2C). Moreover, using allele-specific PCR to specifically detect either the mutant or wild-type sequence for position β770G/T, we confirmed that this mutation was absent in a panel of 100 unrelated human control genomic DNA samples. Additional sequence changes, εC530T and εC1304T, identified in patient 7-1 that did not lead to a change in amino acid sequence or affect splice sites were considered genetic polymorphisms.

Table 2 compares the amino acid sequence for several M1 domains in the region containing the βV229F mutation. It demonstrates that the βV229F mutation occurs in an amino acid residue that is highly conserved in all β subunits of all vertebrate species studied and conserved or substituted conservatively between numerous M1 domains in several nicotinic subunits in other species. This observation indicates that this position may be important for proper channel function.

Functional consequences of the βV229F mutations on the macroscopic response

Dose–response curves were generated to determine the overall consequences of the βV229F mutation (Fig. 3). The dose–response curve for the βV229F mutant was shifted to lower ACh concentrations, with a 10-fold reduction in EC_{50} (5.5 μM) as compared to wild type (54 μM). In addition, we observed a 3.6-fold increase in the normalized macroscopic response for the βV229F mutant (Table 3). The Hill coefficient was not affected by the βV229F mutation, suggesting that the mutation affects channel function without affecting channel cooperativity. Binding of [^{125}I] α-bungarotoxin to surface receptors showed no changes in AChR expression produced by the βV229F mutation (Table 3), indicating normal assembly and oligomerization of the βV229F AChR.

Single-channel studies

To investigate the molecular basis and mechanistic consequence of the βV229F mutation, we recorded single-channel currents in the cell-attached configuration at −100 mV and 4 μM

ACh from oocytes expressing wild-type and βV229F AChRs (Fig. 4). Table 4 summarizes the single-channel parameters obtained for the AChRs studied. Single-channel currents elicited at 4 μM ACh demonstrated that the mutation βV229F significantly increased the channel mean open time constant (11.4 ms) and mean burst duration (20.7 ms) as compared to wild type (Fig. 4 and Table 4). Single-channel amplitude was similar for wild-type (wt) and βV229F AChRs (Fig. 4; Table 4).

To interpret the kinetic behavior of wt and mutant AChRs, we used a simple kinetic model with two open states (see Experimental methods). Fig. 5 shows records of individual bursts and their respective mean open and closed time distribution histograms at 100 μM ACh. We found that, at 100 μM ACh, the βV229F mutation decreased the diliganded closing rate (α_2, 1200) and significantly increased the effective opening rate (β_2 = 33,500 s^{-1}) as compared to wild-type receptors (19,000 $^{s-1}$; Table 5). These changes produced an increase in the effective diliganded open channel equilibrium constants estimated at 100 μM ACh (Θ_2) from 11 in wild-type AChRs to 28 in βV229F AChRs. In addition, we observed a significant reduction in the agonist dissociation constant (700 s^{-1}) as compared to wild type (3600 s^{-1}, Table 5). These results explain the increase in the number of openings per activation episodes from 3 in wild-type to 11 in the βV229F mutation (Figs. 4 and 5). The kinetic analysis of single-channels demonstrated that the greatly prolonged MEPC decay phases recorded in muscle from patient 7-2 can be explained on a molecular level. The perturbed function in βV229F AChRs and, as a consequence, the prolonged MEPC in the patient are due to an increase in the burst length and number of openings per activation episode caused by a reduction in the diliganded closing rate and agonist dissociation constant and an increase diliganded effective opening rate constant (Table 5).

Calcium permeability

Some M1 and M2 domain residues may line the channel pore and determine permeability. To determine if the permeability of the Ca^{2+} was changed in this mutation, we applied the Goldman–Hodgkin–Katz (GHK) constant field model to obtain the permeability ratios from current reversal potentials (Castro and Albuquerque, 1995; Cens et al., 1997). The reversal potentials for wild-type and the mutant receptor were calculated from recordings made with solutions containing a 1 mM and 10 mM Ca^{2+} concentrations. Current–voltage relationships were used to determine the reversal potentials in different solutions (Fig. 6). The relative permeability value of Ca^{2+} with respect to cesium (P_{Ca}/P_{Cs}) in wild-type receptor was 0.37 ± 0.24 (n = 4) which is very similar to values previously reported (Castro and Albuquerque, 1995). The βV229F mutation, however, produced a significant increase in P_{Ca}/P_{Cs} (1.56 ± 0.41) as compared to wild type (0.37 ± 0.24; $P < 0.001$, n = 6; Fig. 6). This greater than 4-fold increase in the preference of the receptor for using Ca^{2+} as a charge carrier correlates well with the marked endplate myopathy seen in this patient. Functionally, the increase in calcium permeability indicates that the βV229F mutation not only contributes to the formation of the pore, but also is involved in determining the ion selectivity of the channel.

Discussion

In the SCS, weakness associated with impaired neuromuscular transmission and prolonged synaptic currents has been attributed to a variety of mutations in different domains of the four subunits forming the muscle AChR (Gomez and Gammack, 1995; Ohno et al., 1995; Sine et al., 1995; Engel et al., 1996; Gomez et al., 1996; Croxen et al., 1997; Milone et al., 1997; Gomez et al., 1998; Croxen et al., 2002; Gomez et al., 2002a). In the present study, we provided the first description of an SCS-associated mutation in the M1 domain of the AChR β subunit. The patient and several members of his family showed slowly progressive muscular weakness. In addition, endplate myopathy was marked by extensive remodeling of the neuromuscular junction (data not shown). In vitro microelectrode studies revealed prolonged low amplitude MEPC in the patient. The clinical and electrophysiological outcomes of the SCS were traced to a kinetic disorder of the AChR attributed to a novel gain-of-function mutation, βV229F, in the M1 domain of the β subunit. Thus, the safety factor for neuromuscular transmission is compromised by a prolonged low amplitude synaptic current resulting from abnormally prolonged single-channel activation episodes.

In vitro expression studies in *Xenopus* oocytes combined with kinetic analysis provided a mechanistic explanation for the consequences of the mutation on the synaptic current. First, we observed that, in whole-cell experiments, mutation βV229F shifted to the left the ACh EC_{50}, when compared to wild type (Table 3). This result, even though indirect (Colquhoun, 1998; Burzomato et al., 2004), suggested that mutation βV229F increased the open probability of the channel. Single-channel analysis at low ACh concentration confirmed our hypothesis. At low ACh concentration, mutation βV229F significantly increases the channel mean open time and, more importantly, the mean burst duration. Kinetic analysis revealed that the gain-in-function produced by mutation βV229F could be explained by a 5-fold reduction in the agonist dissociation constant from the diliganded channel, a decrease in the diliganded closing rate and a 2-fold increase in the effective opening rate compared to wild type. These changes are responsible for an increase in the number of opening per activation episode and the 2.4-fold increase in the effective diliganded open channel equilibrium (Θ_2) in βV229F AChRs.

In SCS, the reduced safety margin of neuromuscular transmission and neuromuscular weakness results from several structural and functional factors that are mostly the consequence of the prolonged synaptic currents. The immediate cause of the prolonged MEPCs is that, during neuromuscular transmission, most AChRs will immediately bind two ACh molecules, and the decay time constant of the MEPC will be approximately determined by the slow component of the burst length distribution at low ACh concentrations. Our analysis indicated that the 5-fold increase in the agonist dissociation constant, the reduction in the channel closing rate and the 2-fold increase in the effective channel opening rate increase the mean burst duration from 2.6 ms in wild-type to 20.7 ms in the βV229F mutation. The increase in mean burst duration calculated from in vitro expression studies correlates well with the decay time constant calculated from MEPC observed in the patient (see Tables 1 and 4). The small difference between the mean burst duration and the decay time of the MEPC observed for the βV229F mutation can be due to an increase in channel desensitization produced by the continuous presence of the agonist in the recording pipette.

Nevertheless, the increase in mean burst duration alone is sufficient to explain the prolonged MEPC observed in the patient.

Prolongation of synaptic currents leads to cation and particularly calcium overload, a stress that may ultimately reduce the amplitude of the MEPCs, by several mechanisms: (1) a decrease in the sodium driving force due to cation overload. This may also affect muscle fiber excitability by causing depolarization block of Na channels; (2) a reduction in the density of AChRs in the endplate because of reduced expression of AChR subunit genes; (3) activation of degradative enzymes leading to the degenerative and remodeling changes of endplate myopathy (see below). In addition, mutant AChRs may have a greater tendency to desensitize, which would lead to further reduction of the MEPC amplitude (Milone et al., 1997). Finally, the observed 40% reduction in the quantal release could significantly reduce MEPCs in the patient. Future experiments using ultrastructural and electrophysiological studies in transgenic mouse models or biopsies of patients bearing this mutation should shed light into the exact mechanism responsible for reduce amplitude of the MEPC.

The pathological hallmark of the SCS is the endplate myopathy, seen only at the electron microscopic level. Endplate myopathy represents a combination of degenerative and remodeling changes of the neuromuscular junction that include widening of the synaptic cleft, degeneration or enlargement of synaptic folds and degeneration of subsynaptic nuclei and mitochondria. These changes have been attributed to overload of the subsynaptic region by cations, principally calcium (Engel et al., 1982; Gomez et al., 2002b). Previous observations have demonstrated that one patient from this kindred manifested a typical endplate myopathy that included pronounced remodeling of the neuromuscular junctional sarcoplasm (Gomez et al., 2002b). As with biopsies of other SCS muscle, calcium deposits were occasionally detected at endplates of this patient. Interestingly, our calcium permeation studies indicate that mutation βV229F produced a significant increase in relative calcium permeability (Fig. 6). This observation suggests that an increase in the preference of the channel to conduct calcium could be a factor contributing to the endplate myopathy observed in the patient. Excessive intracellular calcium accumulation could result in activation of harmful enzymatic and degradative protease pathways that ultimately contribute to the pathology of the disease. In support of this, we were able to demonstrate evidence of deposition of activated caspase enzymes at endplates of this and several SCS patients' muscles (Gomez et al., 2002b).

According to the predicted AChR structure (Miyazawa et al., 2003), position βV229 is located in the upper third portion of the M1 domain. Structural studies have suggested that, at the point where the outer portion of the ion channel pore widens, the M2 domains of the five subunits cannot alone span the larger circumference, implying that a portion of the M1 domain must contribute to the lining of the ion channel (Akabas and Karlin, 1995). Substituted-cysteine-accessibility studies had shown that position βV229 is accessible to solvent in the open state, but not in the resting state of the channel, suggesting that this position contributes to the lumen of the AChR in the open conformation (Zhang and Karlin, 1997). Thus, the significant increase in the preference of the receptor for using Ca^{2+} as a charge carrier in the mutant AChR suggests that position βV229 not only contributes to the formation of the ion channel pore, but is also involved in determining the ion selectivity of

the channel. In addition, our results indicate that mutation βV229F either affects the diameter of the permeation path, the net charge contributing to the driving force or changed the Ca^{2+} binding regions of the pore region.

Comparison with other SCS mutations

To date, 15 different SCS mutations have been discovered in the extracellular, M1 and M2 domains of the AChR (Engel et al., 2003). The kinetic consequences of the SCS mutations vary depending on its localization in the AChR. Accordingly, SCS mutations in the extracellular domain near the acetylcholine binding sites, such as αG153S, act mainly by increasing agonist-binding affinity (Sine et al., 1995), while mutations in the M2 domain (αV249F, βV266M, εL269F, among others) act mainly by slowing down the closing rate constant of the active channel (Ohno et al., 1995; Engel et al., 1996; Milone et al., 1997; Gomez et al., 2002b). Unexpectedly, mutations in the M1 domain (αN217K and εL221F) have been shown to produce the kinetic abnormality underlying the SCS mainly by reducing the agonist dissociation rate constant (Wang et al., 1997; Croxen et al., 2002). These results were surprising given the fact that the positions in which this these mutations are located are some 30 A° away from the agonist's binding sites.

The mutation βV229F described in this study is similar to the other SCS M1 domain mutations in that it reduces the agonist dissociation constant and, as a consequence, increases the number of openings per activation episode (Wang et al., 1997; Croxen et al., 2002). The fact that a mutation in the M1 domain of the AChR β subunit has such an effect on agonist-binding affinity is even more surprising than the results obtained from previous SCS M1 domain mutations. The large effect on the agonist dissociation constant for the diliganded channel observed for the αN217K and εL221F mutations is consistent with the fact that the acetylcholine binding sites are located in the interface between the α–y and α–ε subunits (Karlin, 2002). That is, it is not surprising that perturbations caused by these mutations allosterically propagate to the binding sites and affect agonist-binding affinity. Alternatively, these mutations may be acting even closer by stabilizing the interaction between residues involved in the principal pathway coupling agonist binding to channel gating in the so-called pre-M1 domain region (Lee and Sine, 2005). However, given that the AChR β subunit does not contribute to the formation of the agonist-binding pockets, the structural and functional basis for the produced effect of the βV229F mutation on the agonist dissociation constant remains obscure. The development of a high-resolution crystal structure of the acetylcholine receptor in the different conformational states should help clarify this issue.

Unlike the other SCS M1 domain mutations, the βV229F mutation significantly affects the parameters governing channel gating. It produces a substantial increase in the effective channel opening rate and a reduction in the channel closing rate. Perhaps, the bigger, more hydrophobic phenylalanine substitution enhances gating by creating new interactions with residues in the nearby M2 domain. The perturbation produced by the mutation will then propagate to the proposed channel gate region during channel activation only a couple of amino acids below. Nevertheless, our results indicated a modulatory role of the M1 domain in structures that couple ligand binding to the channel gate.

To summarize, we found that the clinical and electrophysiological outcome of a novel form of the SCS is caused by a βV229F mutation in the M1 domain of the AChR β subunit. The kinetic and permeation studies presented in this work help to explain the consequences of the βV229F mutation on the miniature endplate currents and thus are direct evidence that the βV229F mutation is responsible for compromising the safety margin of neuromuscular transmission in the patient. Furthermore, our results indicated a contribution of position βV229 to channel gating and an apparent allosteric modulation of the binding site. These results highlight the importance of understanding the conformational changes and molecular interaction taking place during the process of agonist binding to channel gating and their contribution to the shape of the synaptic current.

Experimental methods

Genetic analysis of AChR subunit genes

Screening for mutations in the AChR α, β, δ and ε subunit genes was carried out by direct sequence analysis of AChR subunit exons amplified from genomic DNA by polymerase chain reaction (PCR) as described previously (Gomez and Gammack, 1995; Gomez et al., 1996, 2002a). Briefly, primers corresponding to flanking intron sequences (sometimes containing universal 5′ M13 tail sequence) were used to amplify DNA templates for nucleotide sequence analysis. Di-deoxy sequence analysis was carried out using AChR-specific primers or M13 universal primer and analyzed on an automated DNA sequencer (ABI 377, Applied Biosystems). The nucleotide sequence of the entire coding region for the four AChR subunits was determined after the mutations were identified to exclude the presence of additional mutations. To screen for the presence of the nucleotide substitution (βG770T) that codes for the βV229F mutation in a panel of one hundred normal individuals from a DNA panel (Centre d'Etude du Polymorphisme Humain), we used allele-specific PCR with upstream primer β7U (CAT.ACC.CGG.CAC.TAA.CCA.GG), the down-stream primers β7D (GGA.TGC.ATG.GGG.CAA.TGA.c) and β7Dm (GGA.TGC.ATG.GGG.CAA.TGA.a), which give 24-bp PCR products for wild-type and mutant alleles, respectively.

Oocyte expression studies

The homologous βV229F mutation was generated in mouse β subunit cDNA cloned into the vector, pcDNA/3 using site-directed mutagenesis (Quick-change, Strategene, La Jolla, CA). The mutation was confirmed by di-deoxy nucleotide sequence analysis of the entire cDNA. In vitro mRNA transcription was performed as described previously (Gomez et al., 2002a,b).

Cell culture and transfection

For reversal potential studies, human embryonic kidney 293 (HEK-293, Gibco BRL, Carlsbad, CA) cells were maintained in culture at 37°C, 5% CO_2 in DMEM containing 10% FBS and 0.05 mg/ml Gentamicin (Gibco BRL, Carlsbad, CA). Cells were transfected at ~50% confluency using the Effectene transfection reagent (Qiagen, Valencia, CA). For a 25-ml flask, a total amount of 1 μg of DNA was used, the transfection mix was composed of a ratio of 2α:β:ε:δ subunits. Cells expressing mature receptors were selected 36–48 h after

transfection by using magnetic beads (Dynal Biotech, Lake Success, NY) coated with the mAb35 antibody (Tzartos and Lindstrom, 1980). Cells were replated into 60-mm petri dishes, and recordings were performed 18– 24 h after replating.

Voltage clamp recordings

ACh-induced currents were recorded with two-electrode voltage clamp 3 days after mRNA injection with the Gene Clamp 500 amplifier (Axon Instruments, Foster City, CA). Electrodes were filled with 3 M KCl and had resistances of less than 2 MΩ. Impaled oocytes in the recording chamber were perfused at a rate of 0.5 ml/s with MOR-2 buffer [82 mM NaCl, 2.5 mM KCl, 5 mM $MgCl_2$, 1 mM Na_2HPO_4, 5 mM *N*-(2-Hydroxyethyl)piperazine-*N*′-2-ethanesulfonic acid (HEPES) and 0.2 mM $CaCl_2$ (pH 7.4)]. Dose–response curves for each oocyte were held at a membrane potential of −70 mV. Dose– response data were collected and analyzed as described previously (Tamamizu et al., 1999).

[^{125}I]-α-Bungarotoxin binding assay

The expression of nAChR in the oocyte membrane was assayed by assessing the binding of [^{125}I]-α-bungarotoxin (^{125}I-αBT) (Amersham Life Sciences, Arlington Heights, IL) to intact oocytes as described previously (Tamamizu et al., 1999).

Single-channel recordings

Xenopus oocytes were placed in a recording chamber containing a bath solution of 100 mM KCl, 1 mM $MgCl_2$ and 10 mM HEPES (pH 7.2) at 20 to 22°C. The patch pipettes were made of thick-walled borosilicate glass (Sutter Instruments, Novato, CA). Pipettes typically had resistance of 2 –4 MΩ. The pipette solution contained 100 mM KCl, 10 mM HEPES, 10 mM EGTA (pH 7.2) and 4 or 100 μM ACh. All experiments were performed in the cell-attached configuration at a membrane potential of −100 mV (Hamill et al., 1981). Single-channel currents were recorded using an Axopatch 200B patch clamp amplifier (Axon Instruments), filtered at 5 kHz and stored on VHS tapes using a digital data recorder (VR-10B, Instrutech Corp., Mineola, NY). The data traces were played back into a Pentium-III-based computer through a DigiData 1200 interface (Axon Instruments) and digitalized at 50 kHz using the program Fetchex (Axon Instruments). Single-channel events at low ACh concentration (4 μM) were detected with a half-amplitude crossing algorithm (pClamp6). Open and closed time duration distributions were constructed from pClamp6-generated files using a logarithmic abscissa and a squared root ordinate (Sigworth and Sine, 1987) and fitted using the maximum likelihood algorithm with the appropriate number of components using the program pSTAT (Axon Instruments). At 100 μM ACh concentration, all the channels in the pipette are desensitized. However, individual receptors randomly revert to the non-desensitized state and the kinetic behavior of the opened and closed states of only one channel can be measured as a burst of activity. A burst of openings corresponding to a single channel was defined as a series of openings separated by closed intervals greater than some critical duration (τ_{crit}). This duration was taken as the point of intersection of the predominant closed component and the succeeding one in the closed time histogram, as described elsewhere (Bouzat et al., 2000). Single-channel events at 100 μM ACh concentration were detected and idealized with a half-amplitude crossing criterion using the

program QUB (QUB suite, State University of New York, Buffalo). Only bursts that exhibited durations longer than 100 ms and more than 10 openings per burst were used for further analysis. The resulting open and closed time intervals from single patches at 100 μM ACh were analyzed according to the following kinetic scheme using the program MIL (QUB suite, State University of New York, Buffalo).

$$2\mathrm{A}+\mathrm{R}\underset{k_{-1}}{\overset{k_{+1}}{\rightleftharpoons}}\mathrm{A}+\underset{\mathrm{AR}*}{\overset{\alpha_1\uparrow\downarrow\beta_1}{\mathrm{AR}}}\underset{k_{-2}}{\overset{k_{+2}}{\rightleftharpoons}}\mathrm{A_2R}\underset{\alpha_2}{\overset{\beta_2}{\rightleftharpoons}}\mathrm{A_2R}*+\mathrm{B}\underset{k_{-b}}{\overset{k_{+b}^{[A]}}{\rightleftharpoons}}\mathrm{A_2R}*\mathrm{B}$$

In this scheme, R is the receptor, A is ACh, A_2R is the bi-liganded species, AR* and A_2R* are the mono-liganded and bi-liganded open state of the receptor– ligand complex, respectively, B is the block molecule and A2R* is the blocked state of the channel. k_{+1} and k_{+2} are the binding rate constants and k_{-1} and k_{-2} the first and second dissociation rate constants for the first and second site, respectively. α_1 and α_2 are the fast and slow closing rate constants, respectively, and β_1 and β_2 are the open rate constants, respectively. k_{+b} is the blocking rate and k_{-b} is the rate of opening from the blocked state. The dead time used was set to 30 μs. Probability density functions of open and closed durations were calculated from the fitted rate constants and superimposed on the experimental dwell-time histograms (Qin et al., 1996).

Calcium permeability

Recordings from HEK-293 cells were obtained in whole cell configuration with an Axoclamp 200B amplifier and digitized through a Digidata 1320A (Axon Instruments) at 22–23°C. Patch electrodes were as above except with resistances of 2 –4 MΩ. The electrode solution was composed of 145 mM CsCl, 10 mM HEPES and 5 mM 1,2-bis(2-aminophenoxy)ethane-*N*,*N*,*N*′,*N*′-tetra acetate (pH 7.3). Recordings were initiated in extracellular solution containing 150 mM CsCl, 1 mM $CaCl_2$ and 10 mM HEPES (pH 7.3). To determine the reversal potential of the AChRs voltage, ramp protocols were applied while a fast step perfusion system (Warner Instruments, Hamden, CT) applied an extracellular solution containing 100 μM ACh. This protocol was succeeded by repeating the ramp protocol with a solution containing 100 μM ACh. The data were acquired using the pClamp 8 software (Axon Instruments) in a Pentium III personal computer. The value of the reversal potential was determined for the different mutations at 1 mM and 10 mM $CaCl_2$. The calcium permeability was determined by using an extended GHK equation used to calculate the relative ion permeabilities with respect to Cs^+ (Castro and Albuquerque, 1995):

$$\frac{P_{\mathrm{Ca}}}{P_{\mathrm{Cs}}}\frac{[\mathrm{Cs}^+]_O(1-e^{\Delta V_{\mathrm{rev}}F/\mathrm{RT}})}{4\left[\mathrm{Ca}_1^{2+}\right]_O e^{\Delta V_{\mathrm{rev}}F/\mathrm{RT}}(1+e^{\Delta V_{\mathrm{rev1}}F/\mathrm{RT}})^{-1}-4[\mathrm{Ca}_{10}^{2+}]_O(1+e^{\Delta V_{\mathrm{rev10}}F/\mathrm{RT}})^{-1}}$$

Permeability calculations were made using the Mathematica 4.1 (Wolfram Research Inc, Champaign, IL) software. Statistical analyses of these results were made using the StatView (SAS institute Inc, Cary NC) software package.

Acknowledgments

This work was supported by grant RO1 NS33202, RO1 NS36809 (to CMG), S06-GM50695 (to LVR) and RO1 GM56371-5 and GM08102-27 (to JALD). Manuel Navedo was supported by NIH-MBRS Research Initiative to Support Excellence 5R25GM61151), Carlos A. Báez-Pagán was supported by the UPR-AGEP Grant (HDR981746), Luzed Díaz-Pérez by the LSAMP program (NSFHRD-0114586) and Roberto Zayas was supported by Supplement award R01 NS33202-0S1.

References

Akabas MH, Karlin A. Identification of acetylcholine receptor channel-lining residues in the M1 segment of the alpha-subunit. Biochemistry. 1995; 34:12496–12500. [PubMed: 7547996]

Bouzat C, Barrantes FJ, Sine SM. Nicotinic receptor fourth transmembrane domain: hydrogen bonding by conserved threonine contributes to channel gating kinetics. J. Gen. Physiol. 2000; 115:663–672. [PubMed: 10779322]

Burzomato V, Beato M, Groot-Kormlink PJ, Colquhoun D, Sivilotti LG. J. Neurosci. 2004; 24:10924–10940. [PubMed: 15574743]

Castro NG, Albuquerque EX. Alpha-bungarotoxin-sensitive hippocampal nicotinic receptor channel has a high calcium permeability. Biophys. J. 1995; 68:516–524. [PubMed: 7696505]

Cens T, Nargeot J, Charnet P. Ca^{2+}-permeability of muscle nicotinic acetylcholine receptor is increased by expression of the epsilon subunit. Receptor. Channels. 1997; 5:29–40.

Colquhoun D. Binding, gating, affinity and efficacy: the interpretation of structure–activity relationships for agonists and of the effects of mutating receptors. Br. J. Pharmacol. 1998; 125:924–947. [PubMed: 9846630]

Croxen R, Newland C, Beeson D, Oosterhuis H, Chauplannaz G, Vincent A, Newsom-Davis J. Mutations in different functional domains of the human muscle acetylcholine receptor alpha subunit in patients with the slow-channel congenital myasthenic syndrome. Hum. Mol. Genet. 1997; 6:767–774. [PubMed: 9158151]

Croxen R, Hatton C, Shelley C, Brydson M, Chauplannaz G, Oosterhuis H, Vincent A, Newsom-Davis J, Colquhoun D, Beeson D. Recessive inheritance and variable penetrance of slow-channel congenital myasthenic syndromes. Neurology. 2002; 59:162–168. [PubMed: 12141316]

Engel AG, Lambert EH, Mulder DM, Torres CF, Sahashi K, Bertorini TE, Whitaker JN. A newly recognized congenital myasthenic syndrome attributed to a prolonged open time of the acetylcholine-induced ion channel. Ann. Neurol. 1982; 11:553–569. [PubMed: 6287911]

Engel AG, Ohno K, Milone M, Wang HL, Nakano S, Bouzat C, Pruitt JN, Hutchinson DO, Brengman JM, Bren N, Sieb JP, Sine SM. New mutations in acetylcholine receptor subunit genes reveal heterogeneity in the slow-channel congenital myasthenic syndrome. Hum. Mol. Genet. 1996; 5:1217–1227. [PubMed: 8872460]

Engel AG, Ohno K, Sine SM. Sleuthing molecular targets for neuromuscular diseases at the neuromuscular junction. Nat. Rev. 2003; 4:339–352.

Gomez CM, Gammack JT. A leucine-to-phenylalanine substitution in the acetylcholine receptor ion channel in a family with the slow-channel syndrome. Neurology. 1995; 45:982–985. [PubMed: 7538206]

Gomez CM, Ricardo Maselli BS, Lasalde J, Tamamizu S, Cornblath DR, Lehar M, McNamee M, Kuncl RW. A β subunit mutation in the acetylcholine receptor channel gate causes severe slow-channel syndrome. Ann. Neurol. 1996; 39:717–723.

Gomez, C.; Staub, J.; Maselli, R.; Day, J.; Charnet, P.; Cens, T.; Wollmann, R. Soc. Neurosci. Abstr. Vol. 24. Los Angeles, CA: 1998. Novel β and δ subunit acetylcholine receptor mutations in the slow-channel syndrome demonstrate phenotypic variability; p. 484

Gomez C, Maselli R, Vohra B, Navedo M, Stiles J, Charnet P, Schott K, Rojas L, Keesey J, Verity A, Wollmann R, Lasalde-Dominicci J. Novel delta subunit mutation in slow-channel syndrome causes severe weakness by novel mechanisms. Ann. Neurol. 2002a; 51:102–112. [PubMed: 11782989]

Gomez CC, Maselli R, Groshong J, Zayas R, Wollman RL, Cens T, Charnet P. Active calcium accumulation underlies severe weakness in a panel of mice with slow-channel syndrome. J. Neurosci. 2002b; 22:6447–6457. [PubMed: 12151524]

Hamill OP, Marty A, Neher E, Sakmann B, Sigworth FJ. Improved patch-clamp techniques for high-resolution current recording from cells and cell-free membrane patches. Pflugers Arch. 1981; 391:85–100. [PubMed: 6270629]

Hatton CJ, Shelley C, Brydson M, Beeson D, Colquhoun D. Properties of the human nicotinic receptor, and of the slow-channel myasthenic syndrome mutant (L221F, inferred from maximum likelihood fits. J. Physiol. 2003; 547:729–760. [PubMed: 12562900]

Karlin A. Emerging structure of the nicotinic acetylcholine receptors. Nat. Rev. Neurosci. 2002; 3:102–114. [PubMed: 11836518]

Lee WY, Sine SM. Principal pathway coupling agonist binding to channel gating in nicotinic receptors. Nature. 2005; 438:243–247. [PubMed: 16281039]

Milone M, Wang HL, Ohno K, Fukudome T, Pruitt JN, Bren N, Sine SM, Engel AG. Slow-channel myasthenic syndrome caused by enhanced activation, desensitization, and agonist binding affinity attributable to mutation in the M2 domain of the acetylcholine receptor alpha subunit. J. Neurosci. 1997; 17:5651–5665. [PubMed: 9221765]

Miyazawa A, Fujiyoshi Y, Unwin N. Structure and gating mechanism of the acetylcholine receptor pore. Nature. 2003; 424:949–955. [PubMed: 12827192]

Muley, S.; Gomez, C. Congenital myasthenic syndromes. In: Kaminski, H., editor. Disorders of the Neuromuscular Junction. Humana Press; 2002.

Ohno K, Hutchinson D, Milone M, Brengman J, Bouzat C, Sine S, Engel A. Congenital myasthenic syndrome caused by prolonged acetylcholine receptor channel openings due to a mutation in the M2 domain of the ε subunit. Proc. Natl. Acad. Sci. 1995; 92:758–762. [PubMed: 7531341]

Qin F, Auerbach A, Sachs F. Estimating single-channel kinetic parameters from idealized patch-clamp data containing missed events. Biophys. J. 1996; 70:264–280. [PubMed: 8770203]

Sigworth FJ, Sine SM. Data transformations for improved display and fitting of single channel dwell time histograms. Biophys. J. 1987; 52:1047–1054. [PubMed: 2447968]

Sine SM, Ohno K, Bouzat C, Auerbach A, Milone M, Pruitt JN, Engel AG. Mutation of the acetylcholine receptor α subunit causes a slow-channel myasthenic syndrome by enhancing agonist binding affinity. Neuron. 1995; 15:229–239. [PubMed: 7619526]

Tamamizu S, Lee Y, Hung B, McNamee MG, Lasalde-Dominicci JA. Alteration in ion channel function of mouse nicotinic acetylcholine receptor by mutations in the M4 transmembrane domain. J. Membr. Biol. 1999; 170:157–164. [PubMed: 10430659]

Tzartos SJ, Lindstrom JM. Monoclonal antibodies used to probe acetylcholine receptor structure: localization of the main immunogenic region and detection of similarities between subunits. Proc. Natl. Acad. Sci. U. S. A. 1980; 77:755–759. [PubMed: 6153804]

Wang HL, Auerbach A, Bren N, Ohno K, Engel AG, Sine SM. Mutation in the M1 domain of the acetylcholine receptor alpha subunit decreases the rate of agonist dissociation. J. Gen. Physiol. 1997; 109:757–766. [PubMed: 9222901]

Zhang H, Karlin A. Identification of acetylcholine receptor channel-lining residues in the M1 segment of the beta-subunit. Biochemistry. 1997; 36:15856–15864. [PubMed: 9398318]

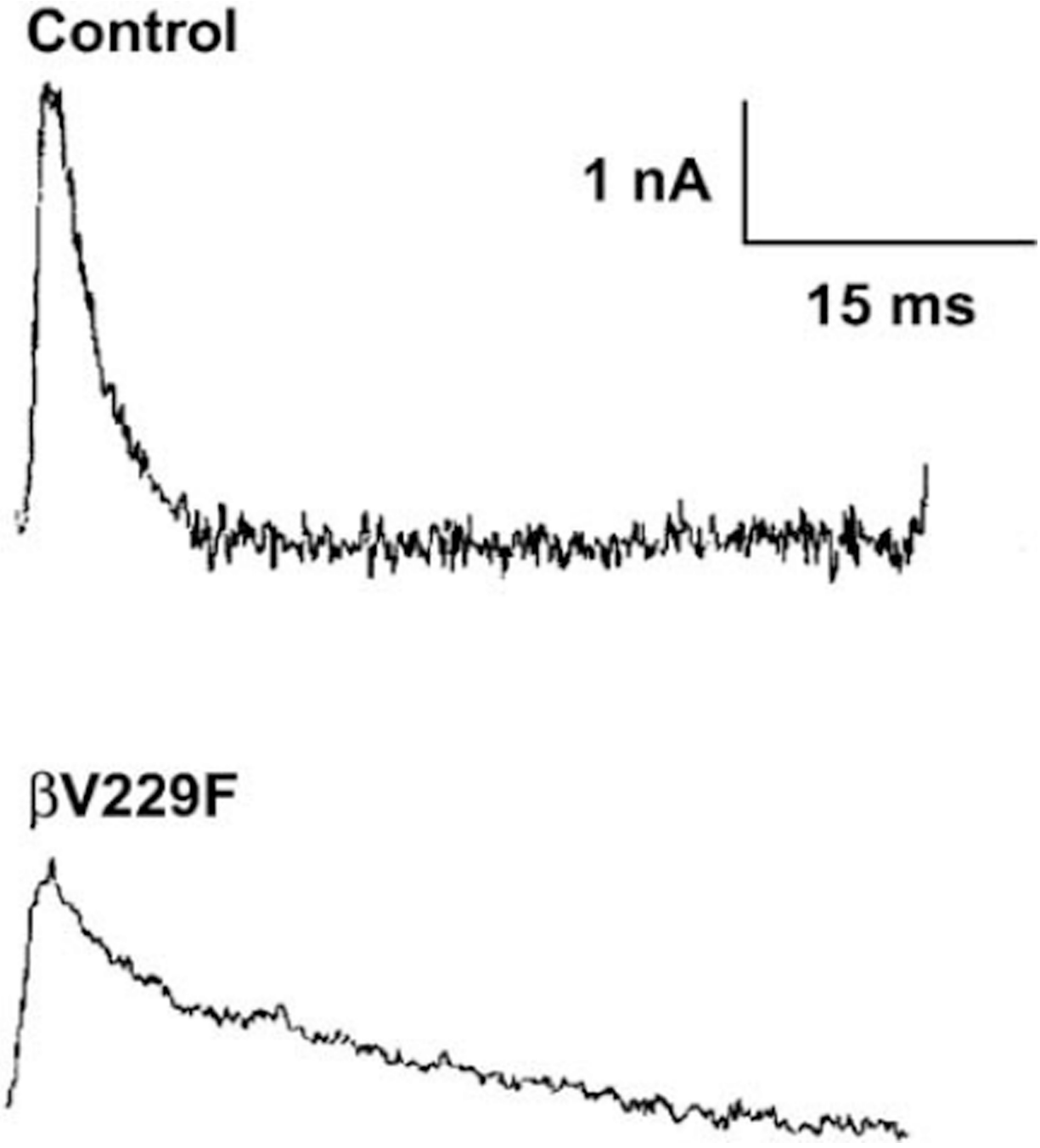

Fig. 1.

Electrophysiological studies. Miniature endplate currents (MEPC) recorded from the anconeus muscle of control and the proband UM:III4. The prolonged miniature endplate current (MEPC) has a bi-exponential decay time constant of 2.3 ms and 26.1 ms, compared with control (3.6 ms).

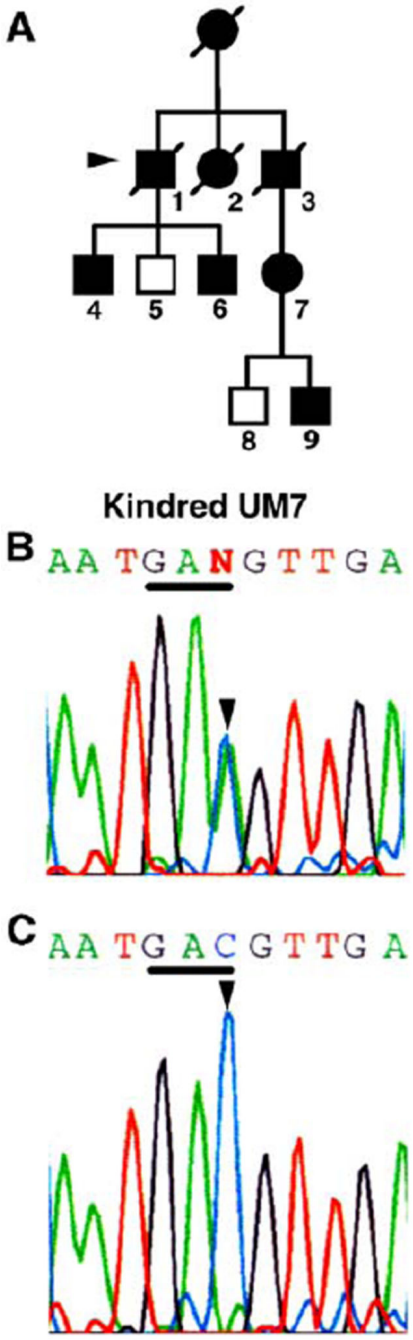

Fig. 2.

Mutations in one kindred with slow-channel syndrome affect a β subunit residues. (A) Pedigree of kindred UM7. Proband 7-1 (arrowhead), his sons, 7-4, 7-6, and niece 7-7 had abnormal electrodiagnostic studies. (B) Genomic sequence of the β subunit encoding the region of the M1 domain *complementary* strand, nucleotides 765– 775, containing the nucleotide position affected in kindred 7. The colored single-letter codes above show the letter N at position 770, where the sequence indicates two nucleotides. Shown is sequence from patient 7-6. One of the parental strands contains a C-to-A (antisense of G-to-T,

arrowhead) substitution, which is present in equivalent abundance to the normal C and which alters the codon GTC to TTC. This mutation occurs at codon V229 and predicts a substitution of a phenylalanine residue. The complementary sequence of codon 229 is underlined. The larger black letters are letter codes for the corresponding amino acids and indicate the position encoding the wild type, valine (V), together with the mutant phenylalanine (F), read in the reverse sequence of the complementary strand. (C) Sequence of the same region obtained from the patient's normal cousin (7–8) containing only a nucleotide C and amino acid valine at this position.

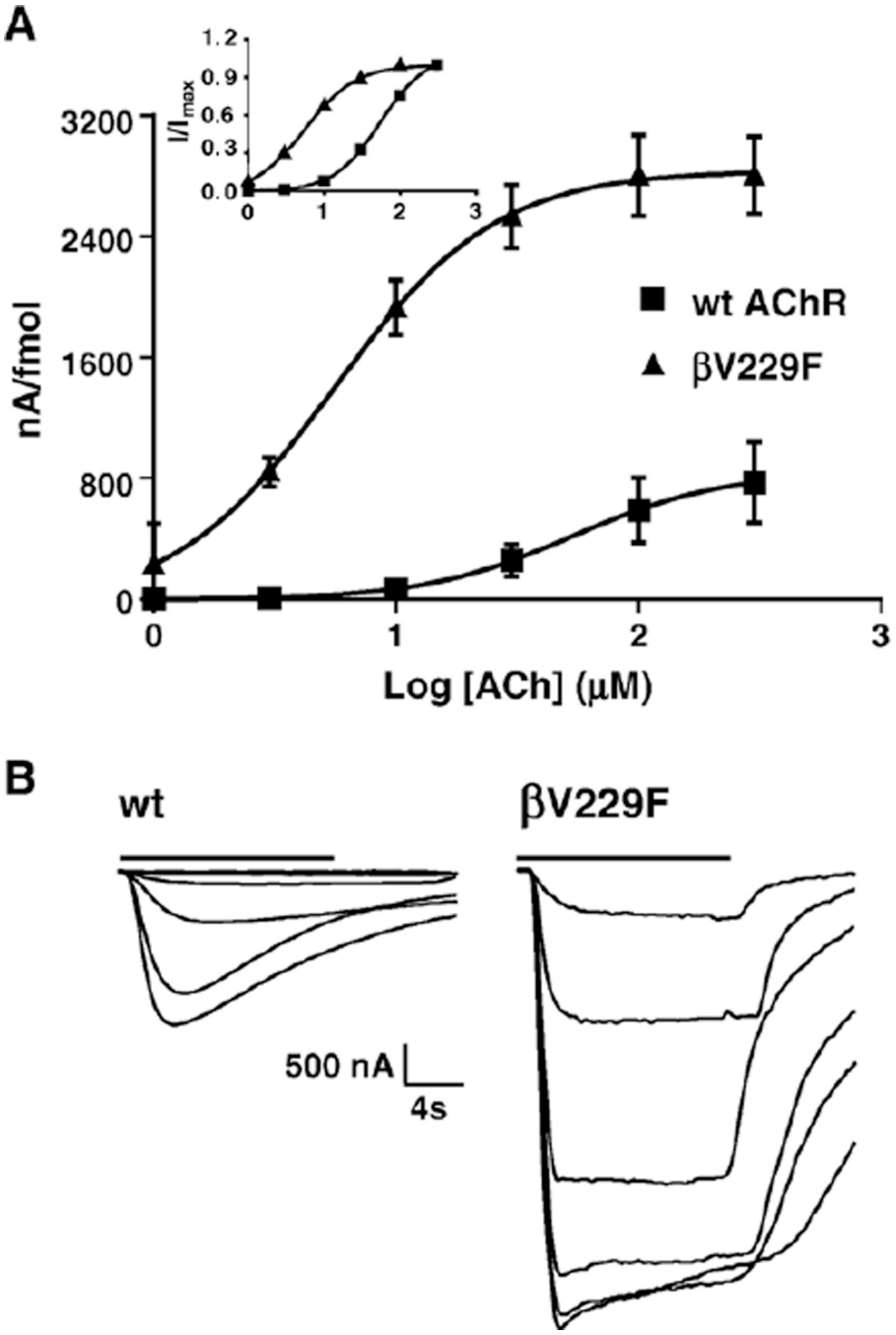

Fig. 3.

Functional consequences of wild-type and βV229F AChR expressed in *Xenopus* oocytes. (A) Dose–response curves from muscle wild-type and βV229F voltage-clamped oocytes. Peak for individual oocytes was obtained from ACh-induced current at 1, 3, 10, 30, 100 and 300 μM ACh. The values at each concentration were averaged, and dose–response curves were reconstructed and normalized to nA per fmol. Inset represents dose–response curves for each of the AChRs tested normalized to maximal response. (B) Representative inward current traces showing normalized ACh-induced current from wild-type and the βV229F

mutation. Bars on top of the macroscopic currents traces represent ACh application. The estimated parameters of the fitted curves are summarized in Table 3.

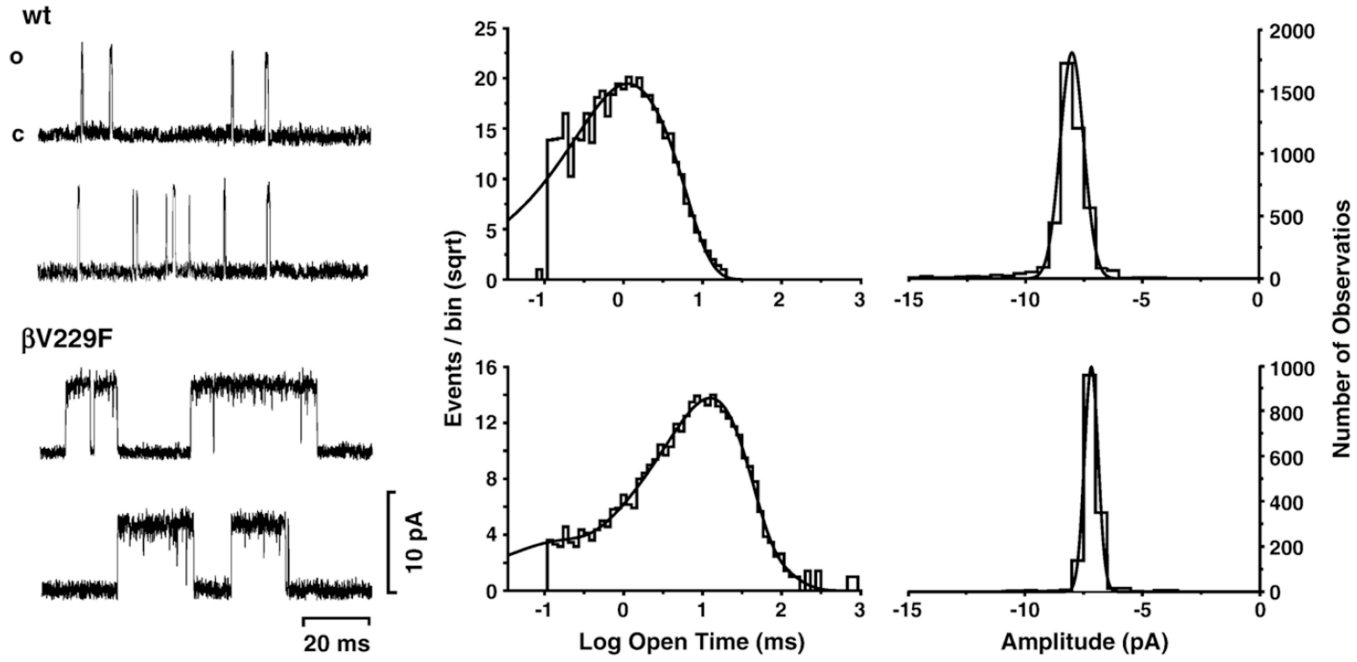

Fig. 4.

Single-channel currents for wild type and βV229F elicited by 4 μM ACh. Currents were recorded from *Xenopus* oocytes expressing either wild-type or the mutant AChRs, as indicated. Center panel, open duration histograms corresponding to the AChRs studied were fitted with exponential functions of the appropriate number of components using the maximum likelihood algorithm. Data were filtered at 5 kHz for each current sample displayed, and channel openings are shown as upward deflections (left panel). Right panel: amplitude histograms. Both wt and mutant AChR show a single amplitude component. All channels were recorded at a holding potential of −100 mV, a sampling rate of 50 kHz and at a temperature of 22°C. Calculated parameters are summarized in Table 4.

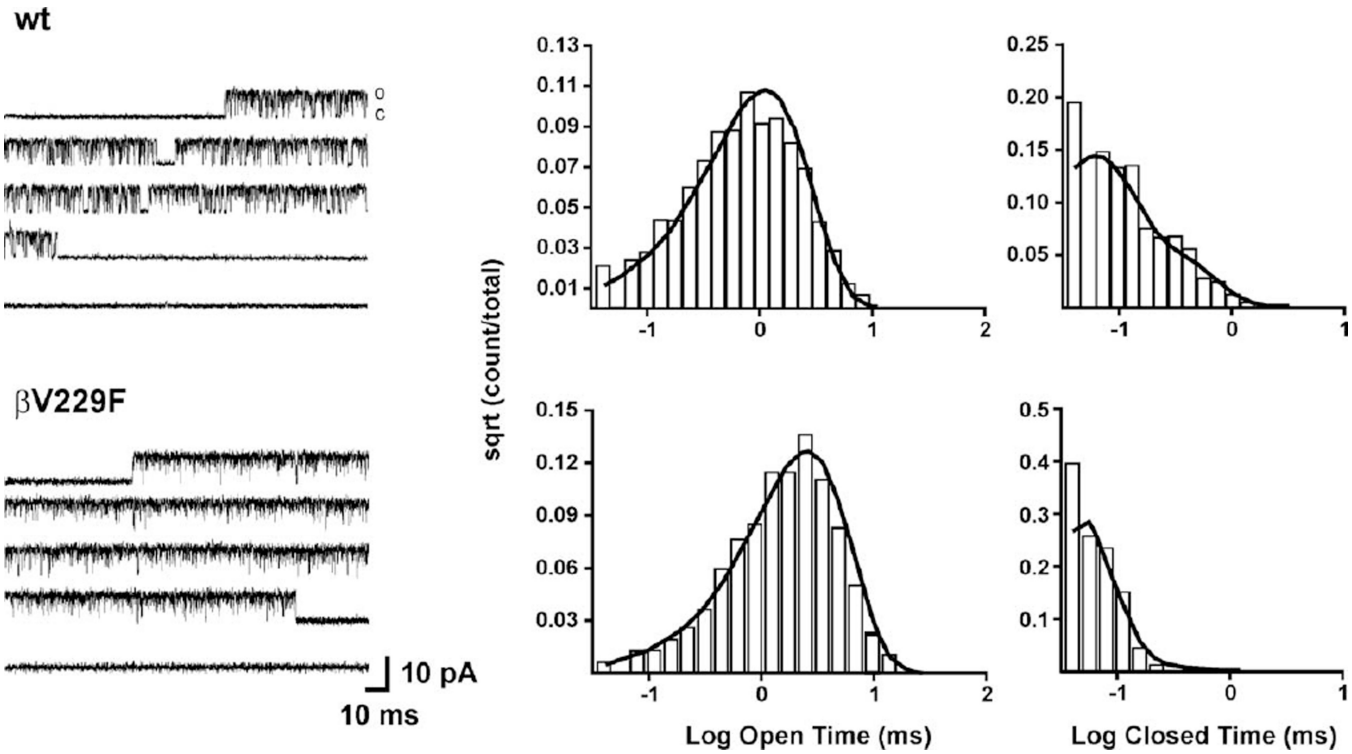

Fig. 5.

Kinetic of activation of wild type and βV229F determined with 100 μM ACh. Currents were recorded from *Xenopus* oocytes expressing either wild-type or the mutant AChRs, as indicated. Corresponding histograms of open and closed durations with superimposed probability density functions for scheme 1 (see Experimental methods) of receptor activation at 100 μM ACh. Table 4 shows the fitted rate constants. Data were filtered at 5 kHz for each current sample displayed and channel openings shown as upward deflections (left side panel). Each current trace represents continuous single-channel current recordings corresponding to bursts of activity for each of the AChRs tested. All channels were recorded at a holding potential of −100 mV, sampling rate of 50 kHz and at a temperature of 22°C.

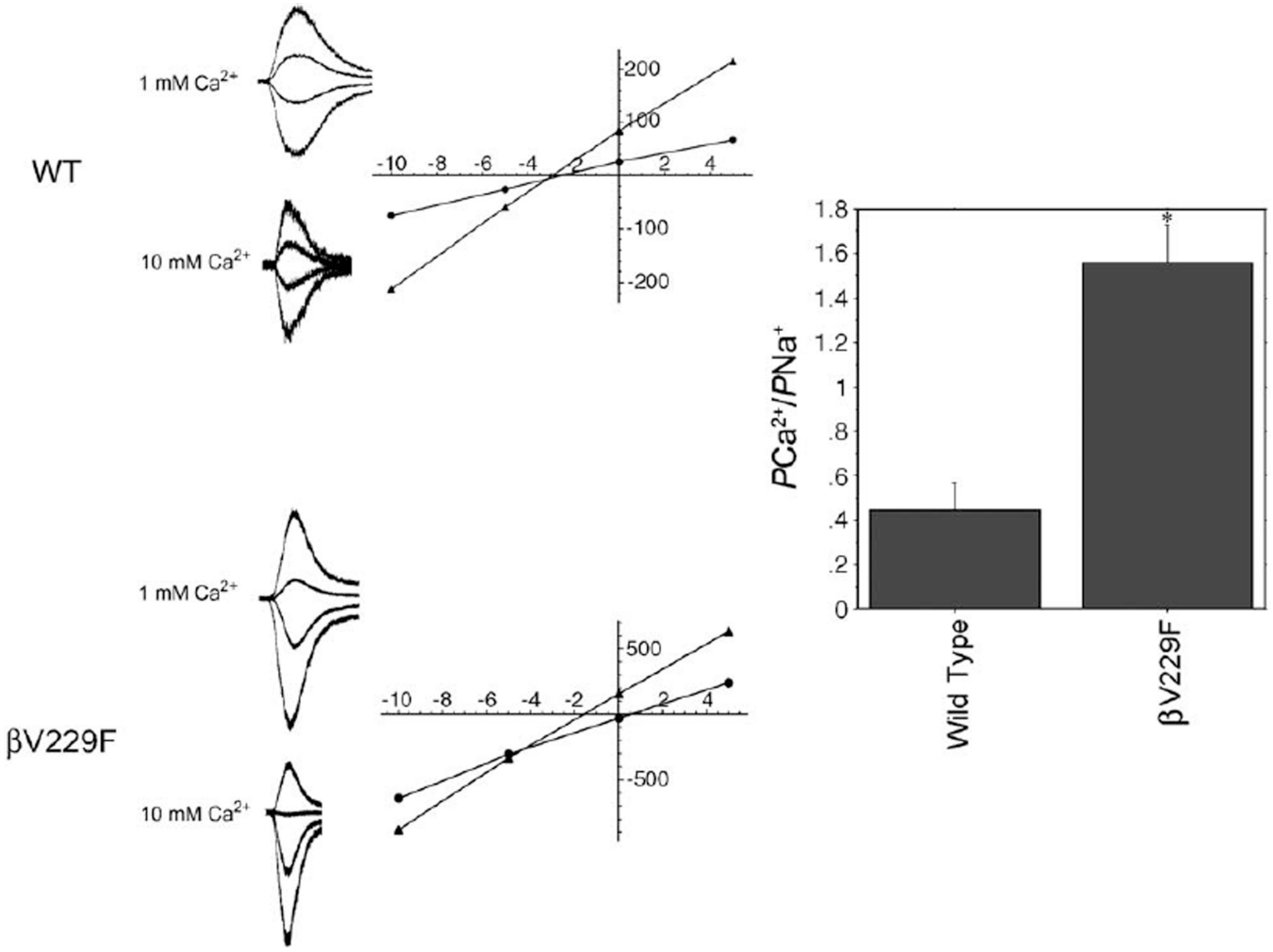

Fig. 6.

M1 mutations in SCCMS differentially affect calcium permeability. (A) Whole-cell current traces elicited over a range of holding potentials (−10 mV to +15 mV, with 4 representative traces shown) in HEK-293 cells expressing AChRs bearing mutation βV229F in the presence of 1 mM (left) or 10 mM (right) Ca^{2+}. (B) Current –voltage relationships used to determine reversal potentials. (C) Relative permeability (P_{Ca}/P_{Cs}) for wild-type or βV229F AChRs computed using reversal potentials and an extended Goldman– Hodgkin–Huxley equation as described in Experimental methods. The value of P_{Ca}/P_{Cs} obtained for βV229F AChRs, 1.56 ± 0.41 (n = 6), was significantly greater than that of wild type, 0.37 ± 0.24 (n = 4, $P < 0.001$, mean ± SD).

Table 1

Serial microelectrode studies of neuromuscular transmission in the slow-channel syndrome

Measurements	Control	UM:III4
MEPP amplitude (mV)	0.8 ± 0.04 (*n* = 82)	0.7 ± 0.3 (*n* = 16)
EPP QC (1 Hz)	22.6 ± 3.0 (*n* = 16)	13.8 ± 4.8 (*n* = 14)
MEPC amplitude (nA)	4.6 ± 0.3 (*n* = 11)	1.8 ± 0.4 (*n* = 6)
MEPC decay time	3.6 ± 0.2 (*n* = 11)	τ_1 = 2.3 ± 1.4 (*n* = 6)
constant (ms)		τ_2 = 26.1 ± 5.0 (*n* = 6)
MEPC frequency		6.4 ± 4.4 (*n* = 10)

Values are given as mean ± SEM. Numbers in parenthesis indicate numbers of EP examined.

Table 2

Multiple alignment sequences of the AChR M1 domain

Human subunits M1 domain			
α1	PLYFIVN	V	IIPCLLFSFLTGLVFYLPT
β1	PLFYLVN	V	IAPCILITLLAIFVFYLPP
δ	PLFYIIN	I	LVPCVLISFMVNLVFYLPA
ε	PLFYVIN	I	IVPCVLISGLVLLAYFLPA
α2	PLFYTIN	L	IIPCLLISCLTVLVFYLPS
α3	PLFYTIN	L	IIPCLLISFLTVLVFYLPS
α4	PLFYTIN	L	IIPCLLISCLTVLVFYLPS
α7	TLYYGLN	L	LIPCVLISALALLVFLLPA
β2	PLFYTIN	L	IIPCVLITSLAILVFYLPS
β4	PLFYTIN	L	IIPCVLTTLLAILVFYLPS
β1	PLFYLVN	V	IAPCILITLLAIFVFYLPP
Patient		F	
β1 subunits M1 domain			
Xenopus	PLFYIVN	V	IVPCILITILAIFVFYLPP
Mouse	PLFYLVN	V	IAPCILITLLAIFVFYLPP
Rat	PLFYLVN	V	IAPCILITLLAIFVFYLPP
Bovine	PLFYLVN	V	IAPCILITLLAIFVFYLPP
Human	PLFYLVN	V	IAPCILITLLAIFVFYLPP
Patient		F	

Table 3

Functional consequences of SCCMS mutations

AChR type (αβδε)	Expression level (fmol)	EC_{50} (μM)	Hill coefficient	Normalized response (−nA/fmol
Wild type	2.3 ± 0.5	54 ± 1	1.4 ± 0.5	800 ± 300
βV229F	1.4 ± 0.4	5.5 ± 1*	1.3 ± 0.5	2800 ± 700*

Values are given as the mean ± SEM. Normalized peak channel activity for individual oocytes was obtained by dividing the ACh-induce current at 300 μM by the fmol of AChR expressed on each oocyte. AChR expression levels, EC_{50}, Hill coefficients and normalized responses were calculated using 7 – 13 oocytes.

* $P < 0.05$.

Table 4

Single-channel recording of wt and mutant AChRs expressed in *Xenopus* oocytes]

AChR	[ACh] (μM)	Patches/events[a]	τ_{o1} (ms)	Fraction	τ_{o2} (ms)	Fraction	σ(pA)	τ_B (ms)
wt	4	3/6996	0.591	0.335	1.59	0.665	7.9 ± 1.0	2.60 (0.68)
βV229F	4	14/3420	0.092	0.038	11.4	0.925	7.2 ± 0.3	20.7 (0.92)

Single-channel currents were recorded in cell-attached patches at a holding potential of −100 mV, temperature at 22°C and at a sampling rate of 50 kHz.

[a]Number of patches/number of events. σ represent AChR single-channel amplitude in pA. τB represents mean burst duration.

Table 5

Kinetic parameters of wt and mutant AChRs expressed in *Xenopus* oocytes

AChR	Events	Bursts	τ_o (ms)	*f*	τ_c (ms)	*f*	k_{-2}	β_2	α_2	Θ_2	P_o
wt	18,736	50	1.0	0.93	0.05	0.58	3600 ± 200	19,000 ± 400	1700 ± 25	11	0.86
βV229F	25,986	77	1.6	0.91	0.03	0.94	700 ± 64	33,500 ± 300	1200 ± 16	28	0.96

Single-channel currents were recorded in cell-attached patches at a holding potential of −100 mV, temperature at 22°C and at a sampling rate of 50 kHz. Θ is the diliganded channel open equilibrium constant. This constant corresponded to ratios of opening and closing diliganded rate constants. Values are the result of fitting scheme 1 to the data obtained at 100 μM ACh. Rate constant are in s^{-1}.